A&A, 706, L6 (2026)
https://doi.org/10.1051/0004-6361/202558046

Astronomy & Astrophysics

LETTER TO THE EDITOR

First direct electron temperature measurement in [O II] zone in I Zw 18

I. A. Zinchenko[1,2,⋆], J. M. Vílchez[3], C. Kehrig[3,4], P. Papaderos[5], and J. E. Méndez-Delgado[6]

[1] Astronomisches Rechen-Institut, Zentrum für Astronomie der Universität Heidelberg, Mönchhofstraße 12-14, D-69120 Heidelberg, Germany
[2] Main Astronomical Observatory, National Academy of Sciences of Ukraine, 27 Akademika Zabolotnoho St., 03143 Kyiv, Ukraine
[3] Instituto de Astrofísica de Andalucía (CSIC), Apartado 3004 18080 Granada, Spain
[4] Observatório Nacional/MCTIC, R. Gen. José Cristino, 77, 20921-400 Rio de Janeiro, Brazil
[5] Instituto de Astrofísica e Ciências do Espaço, Universidade do Porto – CAUP, Rua das Estrelas, PT4150-762 Porto, Portugal
[6] Instituto de Astronomía, Universidad Nacional Autónoma de México, Ap. 70-264, 04510, CDMX, Mexico

Received 10 November 2025 / Accepted 12 January 2026

ABSTRACT

We present new precise measurements of the electron temperatures and oxygen abundances in the southeast knot of I Zw 18, one of the most metal poor blue compact dwarf galaxies known. We used spectroscopic data from the Dark Energy Spectroscopic Instrument Data Release 1 (DESI DR1). For the first time in I Zw 18, we directly measured the electron temperature in the low-ionization zone using the rarely detected [O II]$\lambda\lambda$7320,7330 doublet. We also detected the [O III]λ4363 and [S III]λ6312 auroral lines, which are associated with high- and intermediate-ionization zones, respectively. We derived T_e([O III]) = 21 200 ± 860 K, T_e([O II]) = 16 170 ± 950 K, and T_e([S III]) = 17 290±1750, which highlights a significant temperature difference between the ionization zones. Using these direct temperature measurements, we determined a total oxygen abundance of 12+log(O/H) = 7.066 ± 0.046, log(N/O) = –1.509 ± 0.097, and log(S/O) = –1.558 ± 0.041. Our results extend the calibration of $t_2 - t_3$ relations to the highest temperatures and provide important anchor points for the temperature structure of extremely metal-poor H II regions, including high-redshift galaxies, for which direct temperature measurements are especially challenging.

Key words. ISM: abundances – HII regions – galaxies: abundances – galaxies: dwarf – galaxies: ISM

1. Introduction

Galaxies with extremely low metallicity are rare in the nearby Universe. Nevertheless, they provide exceptional opportunities for studying the physical conditions and processes that occurred in the early Universe and during the epoch of reionization. Therefore, research on these galaxies is crucial to enhance our knowledge of the initial phases of galaxy evolution.

The chemical abundances in H II regions of galaxies are most reliably determined using the direct method (also known as the T_e method). This method relies on the direct measurement of the electron temperature (T_e) using temperature-sensitive auroral lines, such as [O III]λ4363, [N II]λ5755, [S III]λ6312, and [O II]$\lambda\lambda$7320,7330. These auroral lines are very weak and require deep high-quality spectroscopy with large telescopes to be detected. When T_e is determined from the ratio of the auroral to nebular lines and the electron density (n_e) is measured using density-sensitive line ratios, the ion abundances can be computed directly from the observed line intensities using statistical equilibrium equations (see, e.g., Osterbrock & Ferland 2006; Pérez-Montero 2017). For oxygen, which is often used as a gas-phase metallicity tracer, the total abundance is given by O/H = (O^+/H^+) + (O^{++}/H^+), where O^+ is derived from the [O II]$\lambda\lambda$3727,3729 lines and O^{++} from [O III]$\lambda\lambda$4959,5007 lines. For elements such as nitrogen and sulfur, ionization correction factors (ICFs) are essential because N^{++} and S^{3+} cannot be observed in optical spectra; they require correction by ICFs.

In low-metallicity H II regions, very often, the [O III]λ4363 auroral line alone can be measured. It provides an estimate of T_e([O III]), and therefore, of O^{++}/H^+, in the O^{++} zone. In this case, O^+/H^+ in the low-ionization O^+ zone calculates assuming a relation between T_e([O II]) and T_e([O III]). A number of popular linear theoretical relations between T_e in low- and high-ionization zones (also referred as $t_2 - t_3$ relations) based on photoionization models have been proposed by Stasińska (1980), Pagel et al. (1992), Garnett (1992), among others, while others proposed theoretical (Pérez-Montero & Díaz 2003; Izotov et al. 2006) or empirical (Méndez-Delgado et al. 2023) nonlinear relations with a saturation of T_e([O II]) at high T_e([O III]) or even more complex functional relations (Arellano-Córdova & Rodríguez 2020; Rickards Vaught et al. 2025). Because [O II] and [N II] arise from similar low-ionization zones, it is frequently assumed that T_e([O II]) ~ T_e([N II]) (e.g. Izotov et al. 2006; Croxall et al. 2016; Yates et al. 2020; Zurita et al. 2021). Therefore, T_e([N II]) is often used in $t_2 - t_3$ relations instead of T_e([O II]).

Recent James Webb Space Telescope Near-Infrared Spectrograph (JWST/NIRSpec) observations of star-forming galaxies at $z \sim 2$–3 revealed that the T_e([O II])–T_e([O III]) relation at high redshift exhibits a shallower slope than that found for nearby galaxies, although it remains consistent when extremely metal-poor (XMP) systems are included (Cataldi et al. 2025). Overall, the high-temperature regime is sparsely sampled observationally, and it therefore largely relies on model-based relations. Local XMPs therefore provide an important local benchmark to test the universality of this relation across cosmic time.

⋆ Corresponding author: zinchenko@uni-heidelberg.de

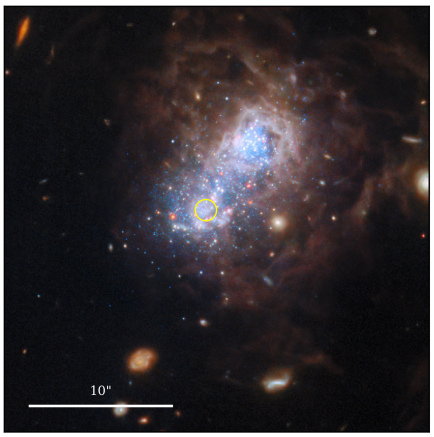

Fig. 1. Color-composite JWST image of I Zw 18 made using four near-IR NIRCam bands (F115W, F200W, F356W, and F444W) by ESA/Webb, NASA, CSA (Hirschauer et al. 2024). North is up, and east is left. The yellow circle represents the spectroscopic 1.5″ aperture of DESI.

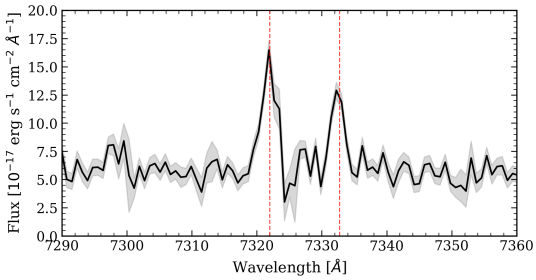

Fig. 2. Rest-frame DESI spectrum of I Zw 18 showing a clear detection of the [O II]$\lambda\lambda$7320,7330 doublet. The gray shadowed area represents the error bars. The dashed vertical lines mark the position of the emission lines.

The system I Zw 18 is a blue compact dwarf (BCD) galaxy that represents one of the most extreme low-metallicity star-forming systems. With an oxygen abundance of approximately 3% of the solar value, corresponding to 12+log(O/H) ∼ 7.1–7.2 (see, e.g., Izotov & Thuan 1998; Vílchez & Iglesias-Páramo 1998; Kehrig et al. 2016), this galaxy serves as a critical laboratory for the examination of physical conditions and processes in the primordial universe and during the very first cycles of star formation. The galaxy actively forms stars with multiple stellar populations that span ages from very young (<30 Myr) to intermediate ages (100–800 Myr). This provides insights into the chemical evolution at different star formation episodes.

Our aim is to obtain the first direct estimate of the electron temperature in the ionization zone of O^+ and the oxygen abundance in I Zw 18 using a new spectrum of its southeast (SE) star-forming (SF) knot published in the Dark Energy Spectroscopic Instrument Data Release 1 (DESI DR1; DESI Collaboration 2025).

2. Data

A new spectrum of the SE knot in I Zw 18 has been published in DESI DR1. Fig. 1 shows the exact position of the DESI aperture, which has a diameter of 1.5″. This corresponds to 138 pc at a distance of 19 Mpc (Fiorentino et al. 2010). Emission line measurements were obtained from FastSpecFit Spectral Synthesis and Emission-Line Catalog, which is designed for stellar continuum and emission-line modeling tailored for DESI (Moustakas et al. 2023). It integrates physically motivated stellar population synthesis and emission line templates to simultaneously model the optical spectrophotometry of DESI from three cameras, alongside ultraviolet to infrared broadband photometry. Along with other data, it provides emission line fluxes and corresponding errors. Table A.1 provides a summary of the emission lines and their fluxes that we used in our analysis. The signal-to-noise ratio in all listed emission lines is >5. Along with the [O III]λ4363 and [S III]λ6312 auroral emission lines, the detection of the auroral [O II]$\lambda\lambda$7320,7330 lines (see Fig. 2) enabled us to make the first direct measurement of the T_e([O II]) in I Zw 18 (see Table 1).

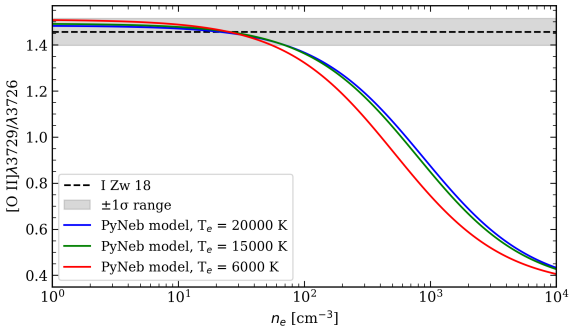

Fig. 3. [O II]λ3729/[O II]λ3726 ratio as a function of n_e. The solid blue line represents the PyNeb model for T_e = 20 000 K, which is typical for extremely low-metallicity H II regions. For comparison, the solid red line represents the PyNeb model for T_e = 6000 K. The dotted line and gray area show the [O II]λ3729/[O II]λ3726 ratio derived from DESI spectrum and its uncertainty.

3. Determining the chemical abundances, electron densities, and temperatures

In this section, we describe the method we used to determine the electron densities (n_e) and temperatures (T_e) along with the chemical abundances. The calculations were performed using the code PyNeb in its version 1.1.24 (Luridiana et al. 2015) with the PyNeb atomic data dictionary PYNEB_23_01.

3.1. Extinction correction and electron density

The Balmer line ratios measured in the DESI spectrum of the SE knot deviate systematically from the theoretical Case B values, particularly for the higher-order Balmer lines. This cannot be explained by dust extinction alone. A more detailed analysis of the Balmer decrement, including the effect of stellar absorption, and suggested flux corrections are presented in Appendix A.

The spectral resolution of the DESI data enabled us to resolve the [O II]$\lambda\lambda$3727,3729 doublet and the [S II]$\lambda\lambda$6716,6731 doublet. For the I Zw 18 SE knot, we calculated line ratios of [O II]λ3729/[O II]λ3726 = 1.456±0.058 and [S II]λ6716/[S II]λ6731 = 1.473±0.066. From these diagnostic ratios, we found that the electron density n_e from [O II]λ3729/[O II]λ3726 is equal to 27±32. The changes in n_e are negligible for T_e > 10 000 K, which is typical for extremely low-metallicity H II regions. Fig. 3 presents a comparison between the observed [O II] doublet flux ratio and theoretical ratios at varying n_e. The figure demonstrates that the theoretical relation between n_e and [O II]λ3729/[O II]λ3726 does not significantly depend on T_e in the low-density regime. The[O II] doublet probes n_e in the O^+ ionization zone, for which we derive T_e and the oxygen abundance below. Because the uncertainty in

Table 1. Electron densities, [O III] temperatures t_3, and element abundances in the I ZW 18 SE knot.

Target ID	n_e([S II]) cm^{-3}	n_e([O II]) cm^{-3}	T_e([O III]) K	T_e([O II]) K	T_e([S III]) K	12+log(O^{++}/H) dex	12+log(O^{+}/H) dex	12+log(O/H) dex
39633324993414901	<100	27±32	21200±860	16170±950	17290±1750	6.924±0.034	6.510±0.075	7.066±0.046

the n_e estimation at low density is substantial, however, we did not use the computed n_e value to determine T_e and the chemical abundances. We instead assumed a fixed value of n_e = 100 cm^{-3} because its effect is negligible in the calculation of the final ionic abundances at low density (Osterbrock & Ferland 2006). Nonetheless, we additionally verified our conclusion in the low-density regime using the [S II]λ6716/[S II]λ6731 ratio and found that the [S II] and [O II] doublets consistently show a low-density state (n_e < 100 cm^{-3}).

3.2. Electron temperatures

From the combination of the nebular [O III]$\lambda\lambda$4959,5007 and auroral [O III]λ4363 lines, we obtained T_e([O III]) = 21 200 ± 860 K. This value is higher than the 19 600 ± 600 K that was reported for the SE knot by Kehrig et al. (2016) and than the averaged T_e = 18 500 ± 2000 K that was measured across the entire galaxy by Rickards Vaught et al. (2025). These two studies both reported significant temperature variations (~15 000–24 000 K) at galaxy scales and locally within its SE knot. Therefore, the slightly elevated value than the averaged estimates by previous IFS studies we obtained from the DESI spectrum is likely caused by the differences in the spatial sampling. T_e(O II) was computed using the [O II]$\lambda\lambda$3729,3726/[O II]$\lambda\lambda$7320,7330 ratio and represents the lower ionization zone. It is significantly lower, T_e([O II]) = 16 170±950 K.

As summarized by Méndez-Delgado et al. (2023), measurements of T_e([O II]) can be variously affected by the uncertainty in the reddening correction or the quality of the flux calibration, the recombination contribution to the collisionally excited lines, temperature fluctuations, or density variations. We corrected the emission line fluxes to make them consistent with the theoretical Balmer decrement, however, and addressed potential issues with reddening and/or flux calibration. Possible temperature fluctuations within the O^+ zone might lead to an overestimate of T_e([O II]). This means that the average temperature in the O^+ zone can be lower than T_e([O II]) and should be considered as an upper limit. Possible density fluctuations will have similar effect. The [O II]λ3729/[O II]λ3726 and [S II]λ6716/[S II]λ6731 ratios indicate a low-density region in the two ionization zones. Although small high-density knots cannot be excluded, their contribution can only lower the average T_e because a higher n_e leads to a lower T_e at a given [O II]$\lambda\lambda$3729,3726/[O II]$\lambda\lambda$7320,7330 ratio.

On the other hand, direct T_e estimates in low-ionization zones at extremely low metallicities are crucial because there are indications that the relation between T_e in zones of high and low ionization is nonlinear. Furthermore, the number of data points with simultaneous measurement of the two temperatures in the T_e([O III]) > 14 000 K range is extremely limited (see, e.g., Arellano-Córdova & Rodríguez 2020; Méndez-Delgado et al. 2023), but it is very important to establish a reliable relation between T_e([O III]) and T_e([O II]) or T_e([N II]) to accurately determine total oxygen abundance and the ICFs for abundances of other chemical elements, which sensitively depend on O^+/O^{++}.

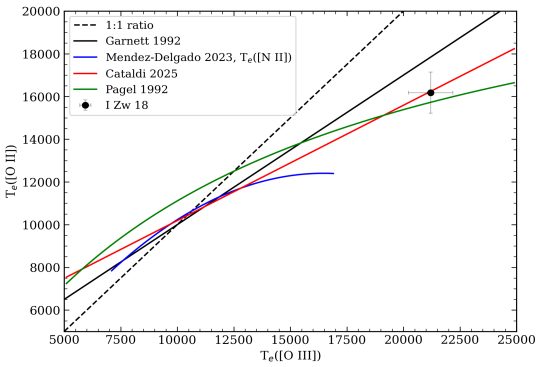

Fig. 4. T_e([O II]) as a function of T_e([O III]) for the model from Garnett (1992) (solid black line) in comparison with T_e([O II]) and T_e([O III]) derived for the SE knot in I Zw 18 (black circle). The solid blue line represents the quadratic model from Méndez-Delgado et al. (2023) for T_e([N II]) as a function of T_e([O III]), and the red and green lines represent the relations from Cataldi et al. (2025) and Pagel et al. (1992), respectively. For this model, we preserved a limited range of T_e([O III]), which represents the range of T_e([O III]) in its calibration sample.

It is interesting to compare our direct T_e([O II]) estimate with the estimate obtained using popular $t_2 - t_3$ relations because they are widely used to calculate the metallicity of metal-poor galaxies when no auroral lines in low-ionization zones are available. The linear $t_2 - t_3$ relation by Garnett (1992) and our estimate of T_e([O III]) gives $T_e^{\rm rel}$([O II]) = 17 840 ± 600 K, which is 16% higher than a direct estimate using the [O II]$\lambda\lambda$7320,7330 lines. This result differs from the conclusion by Méndez-Delgado et al. (2023), who found that T_e([N II]) at high temperature is significantly lower than predicted by linear relations, similar to Garnett (1992). Although the maximum T_e([O III]) in the sampel of Méndez-Delgado et al. (2023) was limited to ~14 000 K, we extend the range to 21200 K with our measurement. The measured T_e([O II]) in I Zw 18 is also relevant for high-redshift SF galaxies, which typically exhibit high ionization parameters and a low metallicity. Some previous studies have shown that the $t_2 - t_3$ relation may depend on the ionization parameter (e.g. Pilyugin 2007; Arellano-Córdova & Rodríguez 2020). In this context, I Zw 18 serves as a local analog of high-z systems. As shown in Fig. 4, our temperature measurements for I Zw 18 are most consistent with the $t_2 - t_3$ relations by Cataldi et al. (2025), which were developed considering high-redshift objects, and with Pagel et al. (1992) based on photoionization models. This indicates that $t_2 - t_3$ relations at high temperatures might be more complex than a one-dimensional relation, and it highlights the need for further studies of the temperature structure at low metallicities.

The detection of the [S III]λ6312 line enabled us to calculate T_e in the medium-temperature [S III] zone, T_e([S III]), because the [S III]λ9531/[S III]λ9069 ratio differs substantially from 2.47, which is the theoretical value. This may indicate telluric absorptions in the [S III]λ9069 line. We therefore only used the [S III]λ9531 nebular line to compute T_e([S III]). We determined T_e([S III]) = 17290±1750 K, which falls between T_e([O II]) and T_e([O III]).

3.3. Chemical abundances

Because we derived T_e directly from the auroral to nebular line ratios in the [O II] and [O III] zones, we estimated the total oxygen abundance using these T_e([O II]) and T_e([O II]) values together with the fluxes of [O II]$\lambda\lambda$3729,3726 and [O III]$\lambda\lambda$4959,5007 assuming a low-density regime. A negligible ionic O^{3+} abundance is expected because the He IIλ4686 line is not detected in the spectrum. Applying the PyNeb *getIonAbundance* method and combining O^+ and O^{++} abundances, we obtained 12+log(O/H) = 7.066 ± 0.046.

Since in previous studies neither the [O II] nor the [N II] auroral lines were measured, the authors relied on the $t_2 - t_3$ relations to estimate O/H. Therefore, we also estimated O/H by computing T_e([O II]) from T_e([O III]) using the $t_2 - t_3$ relation from Garnett (1992). In this case, we obtained 12+log(O/H)$_{t2t3}$ = 7.036 ± 0.035, which is compatible with our estimate using direct measurements of both T_e([O II]) and T_e([O II]). The alternative quadratic $t_2 - t_3$ relation from Méndez-Delgado et al. (2023) only extends to 17 000 K and can therefore not be applied to I Zw 18 without significant extrapolation. Recently, Rickards Vaught et al. (2025) applied three- and two-state models and a parametric $t_2 - t_3$ relation dependent on the excitation parameter and found an oxygen abundance of 7.2 ± 0.02 dex, which is higher by 0.15 dex than our estimate. Thus, different $t_2 - t_3$ relations provide varying estimates of the total O/H, which highlights the need for further studies to better constrain these relations and T_e([O II]) for low-metallicity galaxies.

Assuming $N/O \sim N^+/O^+$ and T_e([O II]) ~T_e([N II]), we obtained the nitrogen-to-oxygen ratio log(N/O) = –1.509 ± 0.097, which is consistent with average value for metal-poor galaxies from Zinchenko et al. (2024). Using the method described by Zinchenko et al. (2024), we also derived log(S/O) = −1.558 ± 0.041. This value is very close to the average S/O ratio for metal-poor galaxies as reported by Zinchenko et al. (2024).

4. Conclusions

We presented the first direct measurement of the electron temperature in the low-ionization zone of I Zw 18, enabled by the detection of the [O II]$\lambda\lambda$7320,7330 auroral doublet in the DESI DR1 spectrum. We found a substantial temperature difference between the ionization zones, with T_e([O III]) = 21 200 ± 860 K exceeding T_e([O II]) = 16170 ± 950 K. This T_e([O II]) value lies between the $t_2 - t_3$ relations proposed by Garnett (1992) and Méndez-Delgado et al. (2023) and provides the first direct T_e([O II]) estimate for very high temperatures. It is far beyond T_e([O III]) ~ 17 000 K, where no empirical $t_2 - t_3$ are calibrated. Using direct temperature measurements for the two ionization zones, we derived 12+log(O/H) = 7.066 ± 0.046. We also derived log(N/O) = –1.509 ± 0.097 and log(S/O) = –1.558 ± 0.041, which are consistent with the average values for metal-poor galaxies from Zinchenko et al. (2024).

Our results extend the calibration of T_e relations to the highest temperatures and provide important anchor points for the temperature structure of extremely metal-poor H II regions. The potential systematic biases in the metallicities derived using empirical or theoretical temperature relations might have important implications for studies of metal-poor galaxies (e.g., the derivation of the primordial helium abundance), including high-redshift galaxies, where direct T_e measurements in [O II] zone are mostly impossible, and the abundance estimates rely on these relations. Accurate chemical abundance determinations in primordial environments therefore require direct T_e measurements in all ionization zones or robust $t_2 - t_3$ relations. This highlights the need for improved models of temperature structures in extremely metal-poor galaxies.

Acknowledgements. We are grateful to the referee for his or her constructive comments. IAZ acknowledges funding from the Deutsche Forschungsgemeinschaft (DFG; German Research Foundation)–project-ID 550945879. JVM acknowledge financial support from the Spanish MINECO grant PID2022-136598NB-C32 and from the AEI "Center of Excellence Severo Ochoa" award to the IAA (SEV-2017-0709). PP acknowledges support by Fundação para a Ciência e a Tecnologia (FCT) grants UID/FIS/04434/2019, UIDB/04434/2020, UIDP/04434/2020 and Principal Investigator contract CIAAUP-092023-CTTI. JEM-D thanks the support of the SECIHTI CBF-2025-I-2048 project "Resolving the Internal Physics of Galaxies: From Local Scales to Global Structure with the SDSS-V Local Volume Mapper" (PI: Méndez-Delgado). This research used data obtained with the Dark Energy Spectroscopic Instrument (DESI). DESI construction and operations are managed by the Lawrence Berkeley National Laboratory. This material is based upon work supported by the U.S. Department of Energy, Office of Science, Office of High-Energy Physics, under Contract No. DE–AC02–05CH11231, and by the National Energy Research Scientific Computing Center, a DOE Office of Science User Facility under the same contract. Additional support for DESI was provided by the U.S. National Science Foundation (NSF), Division of Astronomical Sciences under Contract No. AST-0950945 to the NSF's National Optical-Infrared Astronomy Research Laboratory; the Science and Technology Facilities Council of the United Kingdom; the Gordon and Betty Moore Foundation; the Heising-Simons Foundation; the French Alternative Energies and Atomic Energy Commission (CEA); the National Council of Science and Technology of Mexico (CONACYT); the Ministry of Science and Innovation of Spain (MICINN), and by the DESI Member Institutions: www.desi.lbl.gov/collaborating-institutions.

References

Arellano-Córdova, K. Z., & Rodríguez, M. 2020, MNRAS, 497, 672
Cataldi, E., Belfiore, F., Curti, M., et al. 2025, A&A, 703, A208
Croxall, K. V., Pogge, R. W., Berg, D. A., Skillman, E. D., & Moustakas, J. 2016, ApJ, 830, 4
DESI Collaboration (Abdul-Karim, M., et al.) 2025, ArXiv e-prints [arXiv:2503.14745]
Fiorentino, G., Contreras Ramos, R., Clementini, G., et al. 2010, ApJ, 711, 808
Fitzpatrick, E. L. 1999, PASP, 111, 63
Flury, S. R., Jaskot, A. E., Ferguson, H. C., et al. 2022, ApJ, 930, 126
Garnett, D. R. 1992, AJ, 103, 1330
Hirschauer, A. S., Crouzet, N., Habel, N., et al. 2024, AJ, 168, 23
Izotov, Y. I., & Thuan, T. X. 1998, ApJ, 497, 227
Izotov, Y. I., Thuan, T. X., & Lipovetsky, V. A. 1994, ApJ, 435, 647
Izotov, Y. I., Stasińska, G., Meynet, G., Guseva, N. G., & Thuan, T. X. 2006, A&A, 448, 955
Kehrig, C., Vílchez, J. M., Pérez-Montero, E., et al. 2016, MNRAS, 459, 2992
Luridiana, V., Morisset, C., & Shaw, R. A. 2015, A&A, 573, A42
Méndez-Delgado, J. E., Esteban, C., García-Rojas, J., et al. 2023, MNRAS, 523, 2952
Moustakas, J., Scholte, D., Dey, B., & Khederlarian, A. 2023, Astrophysics Source Code Library [record ascl:2308.005]
Osterbrock, D. E., & Ferland, G. J. 2006, Astrophysics of gaseous nebulae and active galactic nuclei
Pagel, B. E. J., Simonson, E. A., Terlevich, R. J., & Edmunds, M. G. 1992, MNRAS, 255, 325
Pérez-Montero, E. 2017, PASP, 129, 043001
Pérez-Montero, E., & Díaz, A. I. 2003, MNRAS, 346, 105
Pilyugin, L. S. 2007, MNRAS, 375, 685
Rickards Vaught, R. J., Hunt, L. K., Aloisi, A., et al. 2025, ApJ, 990, 111
Scarlata, C., Hayes, M., Panagia, N., et al. 2024, ArXiv e-prints [arXiv:2404.09015]
Skillman, E. D., & Kennicutt, R. C., Jr 1993, ApJ, 411, 655
Stasińska, G. 1980, A&A, 85, 359
Ucci, G., Ferrara, A., Gallerani, S., et al. 2019, MNRAS, 483, 1295
Vílchez, J. M., & Iglesias-Páramo, J. 1998, ApJ, 508, 248
Yates, R. M., Schady, P., Chen, T. W., Schweyer, T., & Wiseman, P. 2020, A&A, 634, A107
Zinchenko, I. A., Sobolenko, M., Vílchez, J. M., & Kehrig, C. 2024, A&A, 690, A28
Zurita, A., Florido, E., Bresolin, F., Pérez, I., & Pérez-Montero, E. 2021, MNRAS, 500, 2380

Table A.1. Emission line fluxes normalized to Hβ = 100.

Line	FastSpecFit [a]	Gaussian fit [b]	Case B[c]	Corr[d]
[O II]λ3726	22.71±0.70			0.88
[O II]λ3729	33.07±0.85			0.88
Hδ	29.73±0.54	30.47±1.18	26.4	0.88
Hγ	52.41±0.72	50.91±0.99	47.5	0.9
[O III]λ4363	6.96±0.43			0.9
Hβ	100.00±0.65	100.00±1.04	100.0	
[O III]λ4959	58.27±0.49			
[O III]λ5007	169.25±0.89			
[S III]λ6312	0.67±0.10			
[N II]λ6548	0.49±0.09			
Hα	264.90±0.95	278.02±2.56	274.6	
[N II]λ6584	1.44±0.09			
[S II]λ6716	3.94±0.11			
[S II]λ6731	2.67±0.10			
[O II]λ7320[e]	0.89±0.08			
[O II]λ7330[f]	0.70±0.06			
[S III]λ9069	3.07±0.07			
[S III]λ9531	9.43±0.13			

Notes. [a]Flux from FastSpecFit VAC. [b]Flux from our Gaussian fit without subtraction of stellar continuum. [c]Recombination line flux expected from Case B. [d]Flux correction coefficient. [e]The line corresponds to unresolved doublet [O II]$\lambda\lambda$7319,7320. [f]The line corresponds to unresolved doublet [O II]$\lambda\lambda$7329,7330.

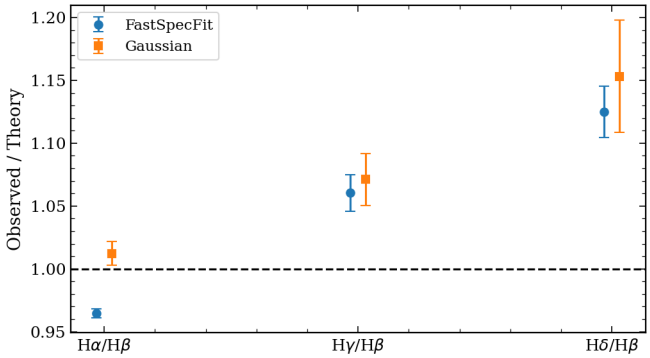

Fig. A.1. Observed-to-theoretical Balmer line ratios (Hα/Hβ, Hγ/Hβ, Hδ/Hβ) for two measurement methods. Blue circles represent full spectral fitting including stellar absorption component from FastSpecFit catalog. Orange squares represent our fitting with single Gaussian without subtraction of stellar continuum. Error bars show 1σ uncertainties, and the dashed line marks the consistency with Case B recombination at n_e = 100 cm^{-3} and T_e = 20 000 K.

Appendix A: Emission line fluxes and correction for extinction

We summarize emission line measurements from the VAC FastSpecFit catalog in Table A.1. The fluxes returned by FastSpecFit are already corrected for Galactic extinction. This table shows that the measured Hα/Hβ ratio (2.649 ± 0.020) is $\simeq$ 3% lower than the theoretical value expected at T_e = 20 000 K, formally yielding a negative c(Hβ) = −0.045 ± 0.009 when applying the extinction curve of Fitzpatrick (1999), while previous studies reported a small positive c(Hβ) values (Skillman & Kennicutt 1993; Vílchez & Iglesias-Páramo 1998; Izotov et al. 1994; Kehrig et al. 2016). Ucci et al. (2019) using the same IFU data as Kehrig et al. (2016), also reported very low but positive visual extinction values, $A_V \sim 0.01$ mag, in most spaxels.

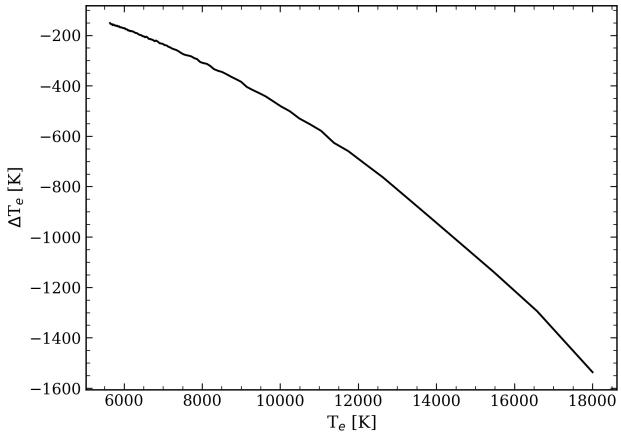

Fig. A.2. Difference in the derived T_e([O II]) caused by a 10% increase in the [O II]$\lambda\lambda$3726,3729 flux as a function of the original temperature.

At the same time, the observed Hγ/Hβ and Hδ/Hβ ratios exceed their theoretical values by ∼ 6–12%, also implying negative c(Hβ). For the physical conditions typical of metal-poor H II regions, we adopt Case B Balmer ratios at n_e = 100 cm^{-3} and T_e = 20 000 K computed with PyNeb. The theoretical ratios used in this work are listed in Table A.1. These Balmer ratios therefore cannot be explained by a physically plausible dust extinction correction alone.

To test whether overestimation of absorption features during stellar continuum modelling can explain these discrepancies, we refit all Balmer emission lines using single-Gaussian profiles without subtracting stellar component. While this brings Hα/Hβ closer to the theoretical ratio, it does not significantly change Hγ/Hβ or Hδ/Hβ, which remain discrepant beyond their uncertainties as shown in Figure A.1. Thus, we conclude that the elevated higher-order Balmer ratios are not caused by the stellar population fitting performed by FastSpecFit.

Thus, we consider a relative flux calibration bias in the blue part of the DESI spectrum as a likely scenario. Although, we cannot rule out possible deviations from the standard Case B assumptions at very high T_e (e.g. Flury et al. 2022; Scarlata et al. 2024). We therefore apply an empirical correction to the blue spectral region, derived from the ratios of the observed to theoretical Hγ/Hβ and Hδ/Hβ values. The resulting correction factors correspond to a reduction of the measured fluxes by ∼ 12% for [O II]$\lambda\lambda$3726, 3729 and ∼ 10% for [O III]λ4363, based on their proximity in wavelength to the relevant Balmer lines.

Applying this correction increases the derived T_e(O II), but lowers T_e(O III), bringing our T_e(O III) estimate for the SE knot into closer agreement with previous IFU-based studies (e.g. Kehrig et al. 2016; Rickards Vaught et al. 2025). Increase of [O II]$\lambda\lambda$3726, 3729 flux by 10% in T_e(O II) range of 14 000–16 000 K results in T_e(O II) uncertainty of 1 000–1 200 K, which is compatible with statistical uncertainty of our T_e(O II) estimation. Figure A.2 demonstrates the effect of a systematic increase in the [O II]$\lambda\lambda$3726, 3729 flux on the derived electron temperature. In this toy model the T_e([O II]) is computed using PyNeb over a range of input ratios [O II] nebular-to-auroral line ratios (25–250). The x-axis shows the T_e for the reference case, while the y-axis shows the temperature difference ΔT_e between the reference case and a 10% increase in [O II]$\lambda\lambda$3726, 3729 flux.